Available online at www.sciencedirect.com
ScienceDirect
European Polymer Journal 43 (2007) 725–742
EUROPEAN POLYMER JOURNAL
www.elsevier.com/locate/europolj

Macromolecular Nanotechnology

Preparation, thermal properties, morphology, and microstructure of phosphorus-containing epoxy/SiO_2 and polyimide/SiO_2 nanocomposites

Ching Hsuan Lin *, Chen Chia Feng, Ting Yu Hwang

Department of Chemical Engineering, National Chung Hsing University, Taichung, Taiwan

Received 20 August 2006; received in revised form 20 November 2006; accepted 11 December 2006
Available online 27 December 2006

Abstract

A phosphorus-containing tri-ethoxysilane (**dopo-icteos**) reacting from the nucleophilic addition reaction of 9,10-dihydro-9-oxa-10-phosphaphenanthrene 10-oxide (**dopo**) and 3-(trieoxysilyl) isocyanate (**icteos**) was synthesized. The structure of **dopo-icteos** was confirmed by ^{1}H, ^{13}C, ^{31}P NMR and IR spectra. A triethylamine catalyzed mechanism for the **dopo-icteos** synthesis was proposed and verified by NMR spectra. The phosphorus-containing epoxy/SiO_2 and polyimide/SiO_2 nanocomposites were prepared from the in-situ curing of diglycidyl ether of bisphenol A (DGEBA)/4,4-diaminodiphenylmethane(DDM)/**dopo-icteos,** and imidization of poly(amic acid) of pyromellitic dianhydride (PMDA)/4,4′-oxydianiline (ODA)/**dopo-icteos**, respectively. The microstructure and morphology were investigated by ^{29}Si NMR, scanning electron microscope (SEM), EDS (Si and P mapping) analysis and atomic force microscope (AFM). The thermal properties, flame retardancy and dielectric properties of the organic–inorganic hybrids were investigated by differential scanning calorimetry (DSC), dynamic mechanical analysis (DMA), limiting oxygen index (LOI), thermal gravimetric analysis (TGA) and dielectric analyzer (DEA).

Keywords: Epoxy; Polyimide; Nanocomposites; Sol–gel; ^{29}Si NMR

1. Introduction

Organic–inorganic hybrids, which exhibit the advantage of both organic and inorganic materials, can be manufactured by (1) intercalated or exfoliated clay approach [1–3], (2) sol–gel procedure [4–15] or (3) reactive POSS technique [16–18]. Among these approaches, sol–gel procedure attracts much attention due to its lower cost and easier procedures. In the sol–gel process, the inorganic phase was generated through hydrolysis and condensation reactions of alkoxide precursors. The most common precursor of sol–gel reaction is the tetraethoxysilane (TEOS). However, the silica network formed by TEOS does not have a good compatibility with polymers, leading to silica domains with large particles and obvious phase separation.

Epoxy resins are the most common materials for printed circuit board because of the advantage of low price, chemical stability and good adhesion.

* Corresponding author. Tel.: +886 4 22840510 407; fax: +886 4 2285 4734.
E-mail address: linch@dragon.nchu.edu.tw (C.H. Lin).

0014-3057/$ - see front matter © 2007 Elsevier Ltd. All rights reserved.
doi:10.1016/j.eurpolymj.2006.12.030

Polyimide, due to its good thermal stability and mechanical properties, is considered one of the most important substrate for electronic applications. Thus, among the silicon-containing organic–inorganic hybrids, polyimide/silica [4–11] and epoxy/silica [12–15] systems are the most common. According to the literature, the compatibility of organic–inorganic phases can be enhanced by introducing coupling agents, where one alkoxide was replaced by a functional group, such as: oxirane [6,12], amino [5,7,8,10] and isocyanate [4,14,15]. In addition to the chemical bonding, a physical bonding, such as hydrogen bonding can also enhance the compatibility of the organic–inorganic phase. In this current work, a new silane coupling (**dopo-icteos**) with amide structure was synthesized from the nucleophilic addition reaction of 9, 10-dihydro-9-oxa-10-phosphaphenanthrene 10-oxide (**dopo**) and 3-trieoxysilylisocyanate (**icteos**). Two phosphorus–silica composites, the epoxy/SiO_2 and polyimide/SiO_2 composites, were prepared from the in-situ curing of (DGEBA)/DDM/**dopo-icteos**, and imidization of poly(amic acid) of PMDA-ODA/**dopo-icteos**, respectively. Since **dopo-icteos** exhibits an amide structure, which can provide hydrogen bonding with hydroxy of epoxy chains or carbonyl of polyimide chains, an improvement in compatibility of organic–inorganic phase are expected. The microstructure, morphology, thermal properties and dielectric properties of the synthesized organic–inorganic hybrids were investigated and discussed.

2. Experimental section

2.1. Materials

Diglycidyl ether of bisphenol A (dgeba) with EEW 187 g/eq was kindly supplied by Nan Ya plastics, Taiwan. Pyromellitic dianhydride (PMDA, Lancaster) was heated at 170 °C overnight before use. Triethylamine, 4,4′-oxydianiline (ODA), 9,10-dihydro-9-oxa-10-phosphaphenanthrene 10-oxide (**dopo**) and 3-(triethoxysilyl) isocyanate (icteos) were purchased from TCI. THF and DMAc were distillated over CaH_2. The other solvents used were commercial products (high-performance-liquid-chromatography-grade) and used without further purification.

2.2. Characterization

Differential scanning calorimetry (DSC) scans were obtained from samples of about 8–12 mg in a nitrogen atmosphere at a heating rate of 20 °C/min by the Perkin–Elmer DSC 7. Thermal gravimetric analysis (TGA) was performed with the Seiko Extar 600 at a heating rate of 20 °C/min under nitrogen atmosphere from 60 °C to 850 °C. Dynamic mechanical analysis (DMA) was carried out by the Perkin-Elmer DMA 7e at a heating rate of 10 °C/min or by Perkin–Elmer Pyris Diamond DMA at a heating rate of 5 °C/min. The storage modulus E′ and tan δ were determined as the sample was subjected to temperature scan mode at a programmed heating rate of 10 °C/min from ambient temperature to 450 °C at a frequency of 1 Hz. The test method was performed by tension mode with a tension ratio at 110%, and the amplitude is 20 μm. The LOI was determined with an Atlas Limiting Oxygen Index Chamber according to the standard procedure (ASTM D-2863-77). The NMR is measured by VARIAN INOVA 600 NMR with chloroform or DMSO-d_6 as the solvent. Dielectric measurements were performed with an Agilent 4291B measurement system at a temperature of 30 °C by the two parallel plate modes at 1 GHz. The applied voltage was 1 V. Before testing, samples ($1 \times 1 \times 0.1$ cm^3) were dried under vacuum at 120 °C for 3 h. The observation of EDS analysis (Si and P mapping) and fracture surfaces, which were prepared under the aid of liquid nitrogen, of the hybrids were performed by the scanning electron microscopy (JEOL, JSM-6700F). AFM analysis was performed by DEIKO SPI3800N after spinning coating on a silicon wafer. The spinning coating was performed by the Synrex SSP-01A spin coater. The preparation of polyimide thin film was performed by the Braive automatic coater. The moisture absorption was calculated as percent weight gain $= [(W/W_0) - 1] * 100$, where W is the weight of sample after absorbing water at 25 °C, and W_0 is the initial weight of sample.

2.3. Synthesis of dopo-icteos

To a four-neck round-bottom flask 3-(triethoxysilyl) isocyanate (icteos) 0.1 mole (24.7 g), **dopo** 0.1 mole (21.6 g), triethylamine 0.4 g and dichloromethane 100 ml were added. The reaction mixture was reacted at 25 °C for 8 h. A white product was obtained after dichloromethane was evaporated by a rotary evaporator. The reaction equation of **dopo-icteos** is shown in Scheme 1.

2.4. Preparation of the epoxy/SiO_2 hybrid system

The mixture containing DGEBA 8 g, 4,4-diaminodiphenylmethane 2.12 g and CH_2Cl_2 is as-

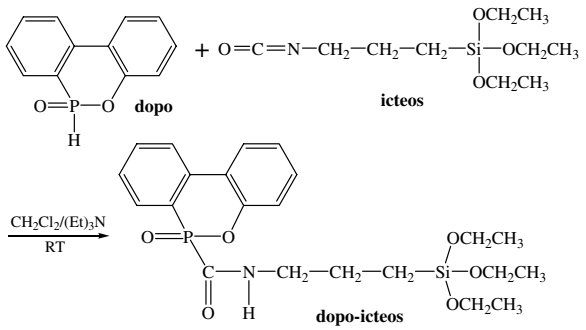

Scheme 1. Synthesis of **dopo-icteos**.

signed as solution A. The mixture containing various amounts of **dopo-icteos** (5, 10, 15 and 20 wt%, respectively, based on weight of DGEBA) and 8 ml CH_2Cl_2 was assigned as solution B. Solutions A and B were stirred at room temperature for 0.5 h. After pouring into a Teflon mold, the mixture was placed at ambient atmosphere to absorb water for 6 h, and then heated at 40 °C (6 h), 100 °C (2 h), 160 °C (4 h) and 180 °C (2 h). The reaction process along with the illustrated microstructure of the epoxy/SiO_2 hybrid is shown in Scheme 2. The sample ID and its corresponding composition are listed in Table 1.

2.5. Preparation of the polyimide/SiO_2 hybrid system

Poly(amic acid) (solid content 15 wt%) of PMDA-ODA was synthesized by the low temperature polymerization of equivalent mole of PMDA

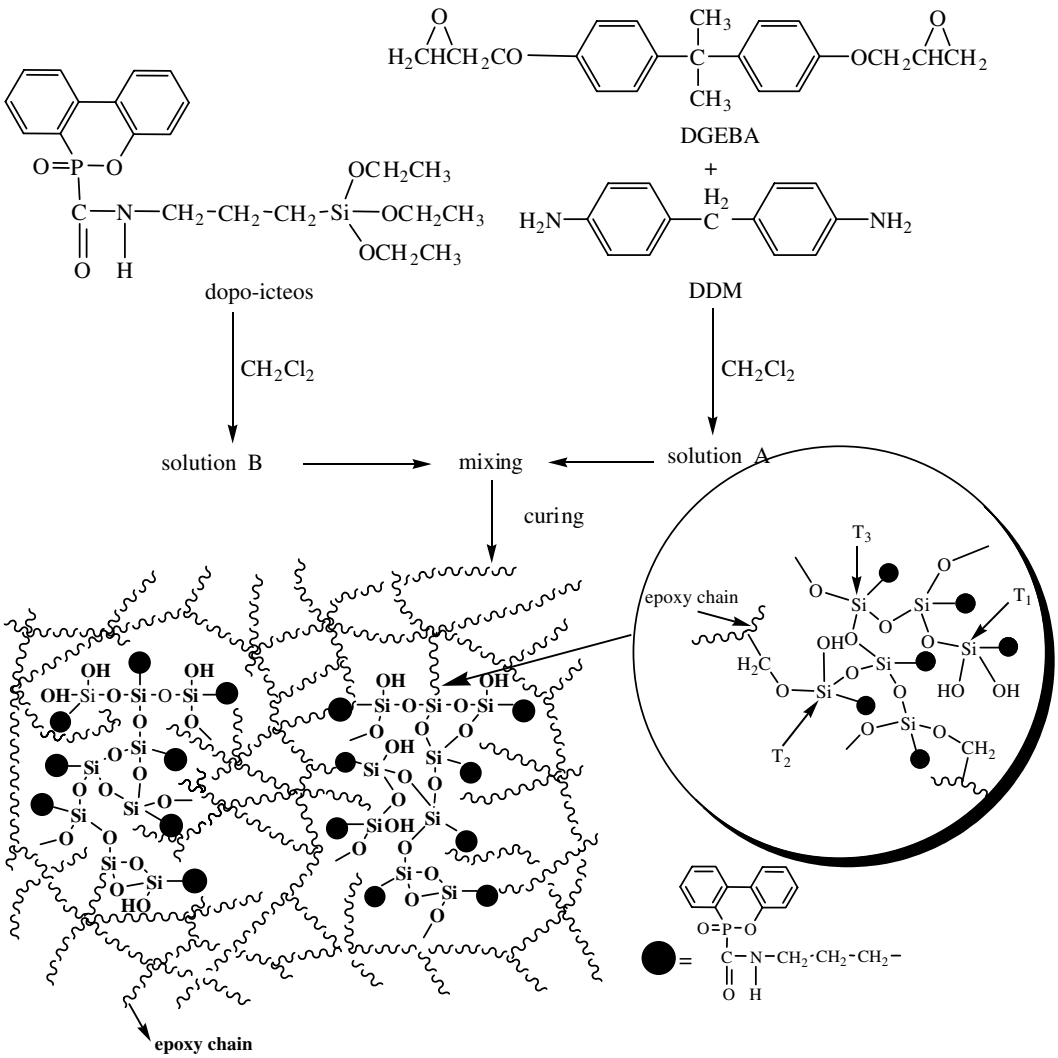

Scheme 2. Synthesis and illustrated microstructure of the epoxy/SiO_2 hybrids.

Table 1
The thermal and dielectric properties of the epoxy/SiO_2 thermosets

Sample ID	**dopo-icteos** (phr)[a]	T_g (°C)[b]	T_d (°C)[c]	Char yield (%)[d]	D_k (U)[e]	D_f (mU)[f]	LOI
Epoxy-di0	0	160	376	15	3.29	70–75.4	21
Epoxy-di5	5	161	344	22	3.27	61–63.6	24
Epoxy-di10	10	163	335	21	3.24	56.8–63	27
Epoxy-di15	15	167	324	25	3.17	54–56.9	28
Epoxy-di20	20	170	322	26	3.16	47–58.1	28

[a] Based on weight of DGEBA.
[b] Measured by DSC.
[c] 5 wt% decomposition temperature (°C).
[d] Residual weight percentage at 800 °C in nitrogen.
[e] Dielectric constant (U) measure at 1 GHz, room temperature.
[f] Dissipation factor (mU) measured at 1 GHz, root temperature.

and ODA in DMAc at 3–5 °C for 2 h. Various amounts of **dopo-icteos** (5, 10, 15, and 20 wt%, respectively, based on the weight of PMDA+ODA) was dissolved in DMAc. The above two solutions were mixed and stirred at room temperature for 0.5 h. After coating on a PET film, the mixture was placed in ambient atmosphere to absorb water for 6 h, and then heated at 60 °C (12 h). After delamination from PET film, the polyimide film was curing at 100 °C (1 h), 200 °C (1 h) and 250 °C (0.5 h) and 300 °C (0.5 h). The reaction process along with the illustrated microstructure of the polyimide/SiO_2 hybrid is shown in Scheme 3. The sample ID and its corresponding composition are listed in Table 2.

3. Results and discussion

3.1. Synthesis of dopo-icteos

A new phosphorus-containing triethyoxysilane, **dopo-icteos**, was synthesized from the nucleophilic addition of **dopo** and **icteos** using triethylamine as a catalyst. Scheme 4 shows the proposed mechanism for the synthesis of **dopo-icteos**. In Scheme 4, triethylamine activated **dopo** by abstracting the active hydrogen of **dopo**, resulting in a **dopo** anion (intermediate I, as shown in Scheme 4). The **dopo** anion then attacks the electron deficient isocyanate of **icteos**, producing the intermediate II. **Dopo-icteos** was formed after the intermediate II abstracts the H^+ from Et_3NH^+. This mechanism can be verified by the NMR spectra of Fig. 1a **dopo** and Fig. 1b **dopo**-triethylamine reaction product, intermediate I ($dopo^-$ Et_3NH^+). Compared with Fig. 1a, Fig. 1b shows a completely different spectrum. The large P–H coupling constant (about 700 Hz) of **dopo** makes the peaks unresolved, so the clear ^1H NMR spectrum of Fig. 1b is resulted from the disappearance of P–H ^1J coupling. This indicates that **dopo** had already reacted with triethylamine. The assignment of each peak in Fig. 1b and c, assisted by the correlations shown in ^1H–^1H COSY and ^1H–^{13}C HETCOR spectra (Fig. 2a and b, respectively), was successfully marked on the figure. This further confirms the formation of intermediate I. The synthesis of **dopo-icteos** can also be monitored by IR spectra. According to the IR trace, the gradual disappearance of isocyanate absorption at 2275 cm^{-1}, and gradual appearance of amide absorption at 1650 cm^{-1} imply the reaction can be complete after reacting for 8 h (not shown here for brief).

3.2. Characterization of dopo-icteos

According to the IR spectrum of **dopo-icteos**, the sharp NH absorption at 3260 cm^{-1}, the aliphatic C–H absorption at around 2929 cm^{-1}, the amide absorption at 1650 cm^{-1}, and the P=O absorption at 1200 cm^{-1} confirm the structure of **dopo-icteos**. However, a Si–OH absorption at 930 cm^{-1} was observed, indicating the hydrolysis of some Si–OR chains. The structure of **dopo-icteos** can also be confirmed by NMR spectra. Fig. 3 shows the ^1H NMR spectrum of **dopo-icteos**. The NH peak at 9.3 ppm, the Ar–H peaks at 7.0–8.3 ppm, the methyl peaks at around 1.1 ppm, and methylene peaks assigned as b, c, d, and e are observed in the figure. A small OH peak at 4.4 ppm for Si–OH resulted from the hydrolysis of Si–OR is observed. Fig. 4 shows the ^{13}C NMR spectrum of **dopo-icteos**. The signals of carbon g split into two peaks because of the P–C ^1J coupling. The peaks of the aromatic carbons at 120–150 ppm, the methyl peaks at around 20 ppm and the methylene peaks assigned as b, c, d, and e are observed in the figure. Fig. 5 shows ^{31}P NMR

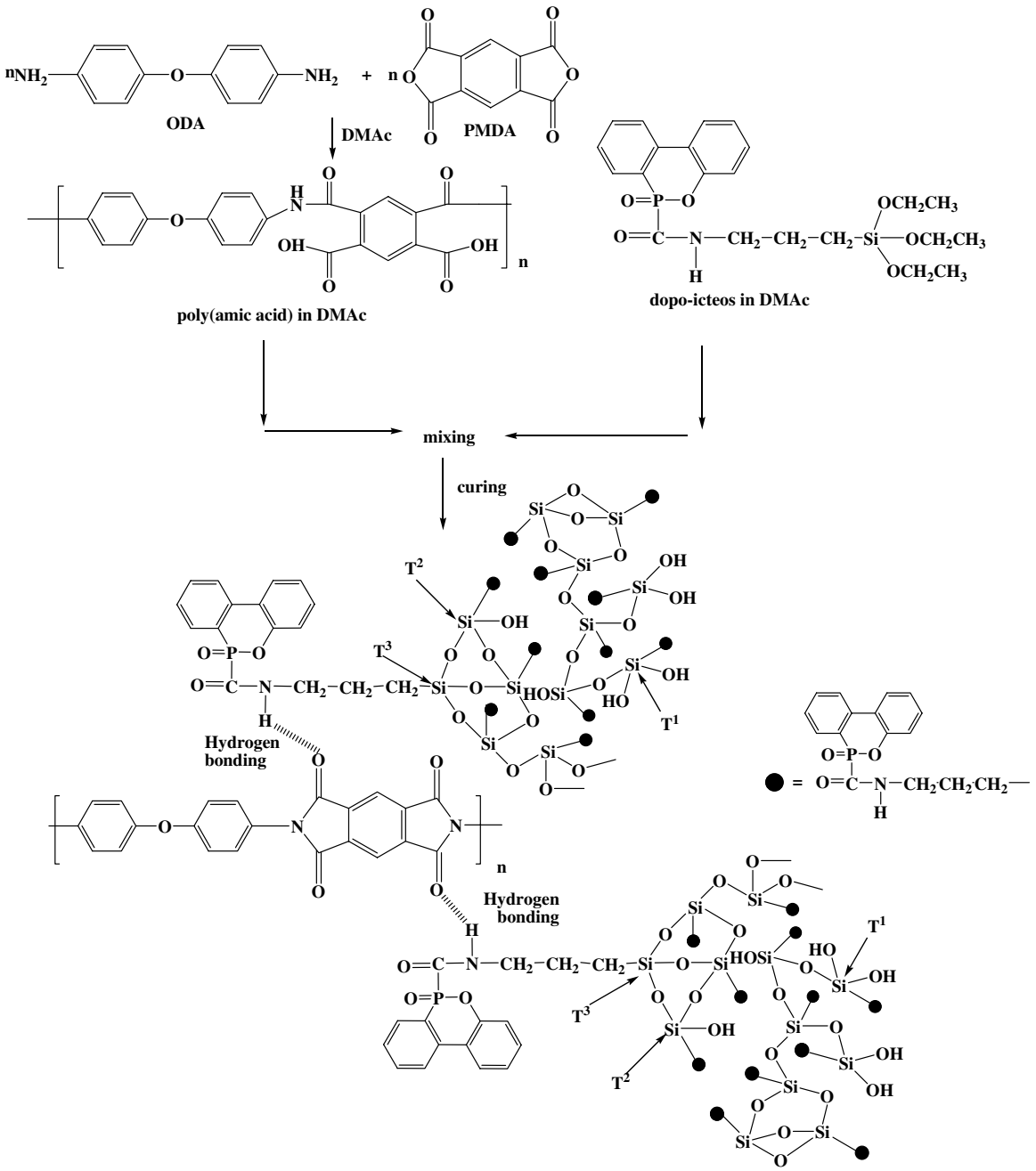

Scheme 3. Synthesis and illustrated microstructure of the polyimide/SiO_2 hybrids.

spectrum of **dopo-icteos**. Besides the major peak at 16.36 ppm, two other peaks at 14.79 and 19.76 ppm are observed. The two small peaks should result from the hydrolyzed **dopo-icteos**, where Si–OR transforms into Si–OH, leading to the phosphorus element has different chemical surroundings.

3.3. ^{29}Si NMR analysis of the epoxy/SiO_2 and polyimide/SiO_2 hybrids

The degree of gel reaction and microstructure of the epoxy/SiO_2 hybrids can be monitored from ^{29}Si NMR Spectra. Fig. 6 shows the solid-state ^{29}Si NMR spectra of the epoxy/SiO_2 hybrids. As shown

Table 2
The thermal stability data of the polyimide/SiO_2 system

Sample ID	**dopo-icteos** (phr)[a]	T_g (°C)[b]	T_g (°C)[c]	Td (°C)[d]	Char yield (%)[e]
pi-di0	0	384	425	585	54
pi-di5	5	380	404	574	58
pi-di10	10	379	394	547	58
pi-di15	15	374	381	521	62
pi-di20	20	372	377	511	63

[a] Based on the weight of PMDA + ODA.
[b] Measured by DMA at a heating rate of 5 °C/min.
[c] Measured by DMA at a heating rate of 10 °C/min.
[d] 5 wt% decomposition temperature (°C).
[e] Residual weight percentage at 800 °C in nitrogen.

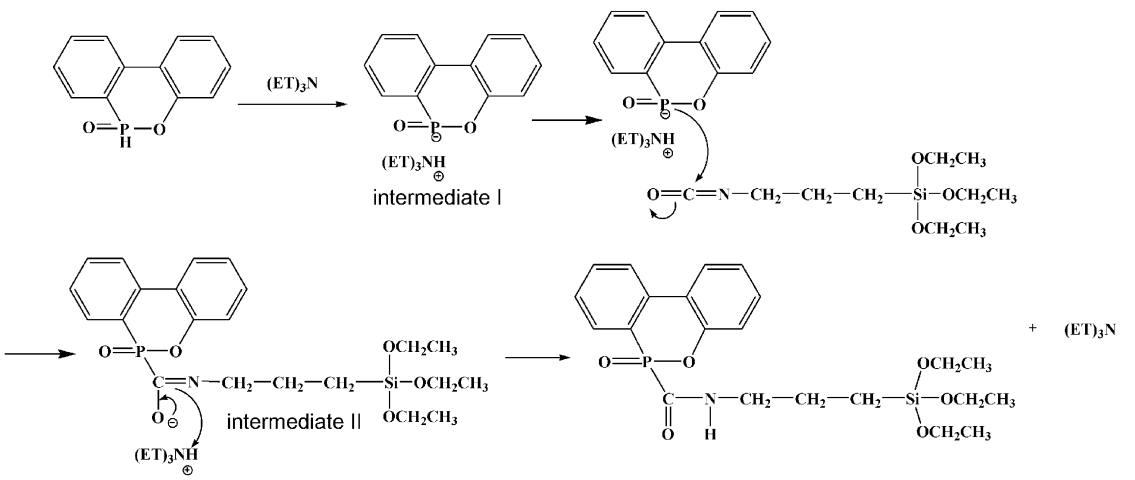

Scheme 4. Proposed mechanisms for the synthesis of **dopo-icteos.**

in Fig. 6, silica network with tri, di and mono-substituted siloxane is designated as T^3 (around −65 ppm), T^2 (around −59.4 ppm) and T^1 (around −48.8 ppm), respectively. According to Fig. 6, tri-substituted siloxane T^3 is the major microstructure in the epoxy/SiO_2 hybrid, suggesting that the conversion of gel reaction is relatively high. For the epoxy/SiO_2 hybrid with a higher **dopo-icteos** content, such as epoxy-di20, a shoulder at $\delta = 54.1$ ppm is observed. The peak might be corresponding to the structure resulting from the dehydration reaction between the hydroxy (C–OH) and silanol (Si–OH) groups [13,19,20], as shown in Scheme 5. Fig. 7 shows the solid-state ^{29}Si NMR spectra of the polyimide/SiO_2 hybrid. Again, as shown in Fig. 6, silica network with tri, di and mono-substituted siloxane is designated as T^3 (around −67 ppm), T^2 (around −59 ppm) and T^1 (around −50 ppm), respectively. The area ratio of T^3/T^2 or T^3/T^1 in the polyimide/SiO_2 is much higher than that in the epoxy/SiO_2 system, indicating that the conversion of gel reaction of the polyimide/SiO_2 system is much higher than that of the epoxy/SiO_2 system. The higher conversion of gel reaction may be due to the higher imidization temperature of the polyimide/SiO_2 system.

3.4. DSC and DMA analysis

Fig. 8 shows the DSC analysis of the epoxy/SiO_2 hybrids. The Tgs of the epoxy/SiO_2 hybrids are in the range of 156–167 °C, increasing slightly with the content of **dopo-icteos**. Generally speaking, Tg may be depressed due to the plasticizing effect of aliphatic bonds [21]. Thus, the Tg-enhanced effect of the epoxy/SiO_2hybrids can be explained by the restriction of chain motion due to the formation of silica network [13]. The dehydration reaction between the hydroxy and silanol (Scheme 5) groups also reduce the mobility of epoxy network. Furthermore, the bulky biphenylene-phosphinate side group

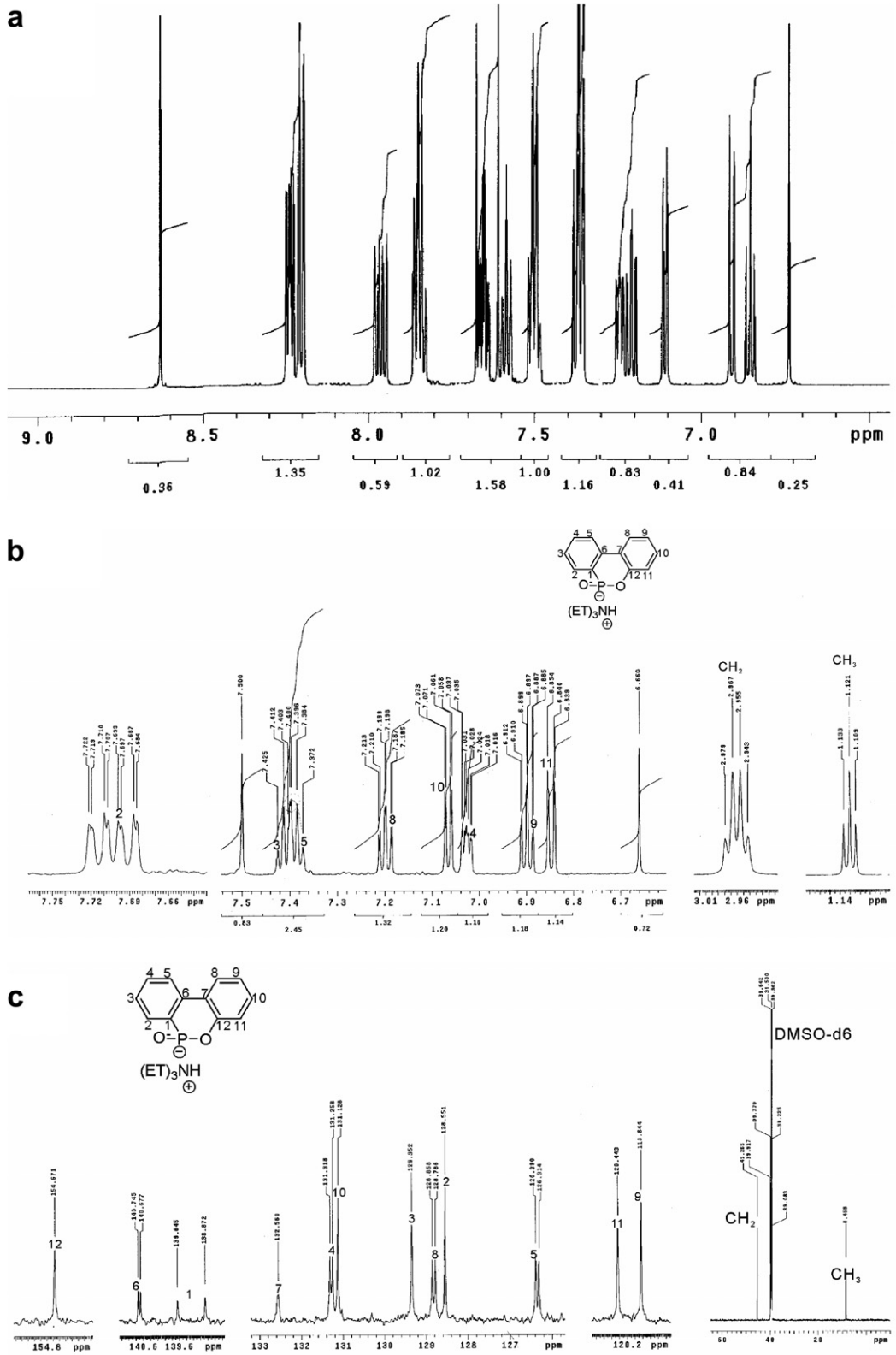

Fig. 1. (a) ^{1}H NMR spectrum of **dopo**, (b) ^{1}H NMR and (c) ^{13}C NMR spectra of **dopo**-triethylamine reaction product, the intermediate I (**dopo**$^{-}$$Et_3NH^{+}$).

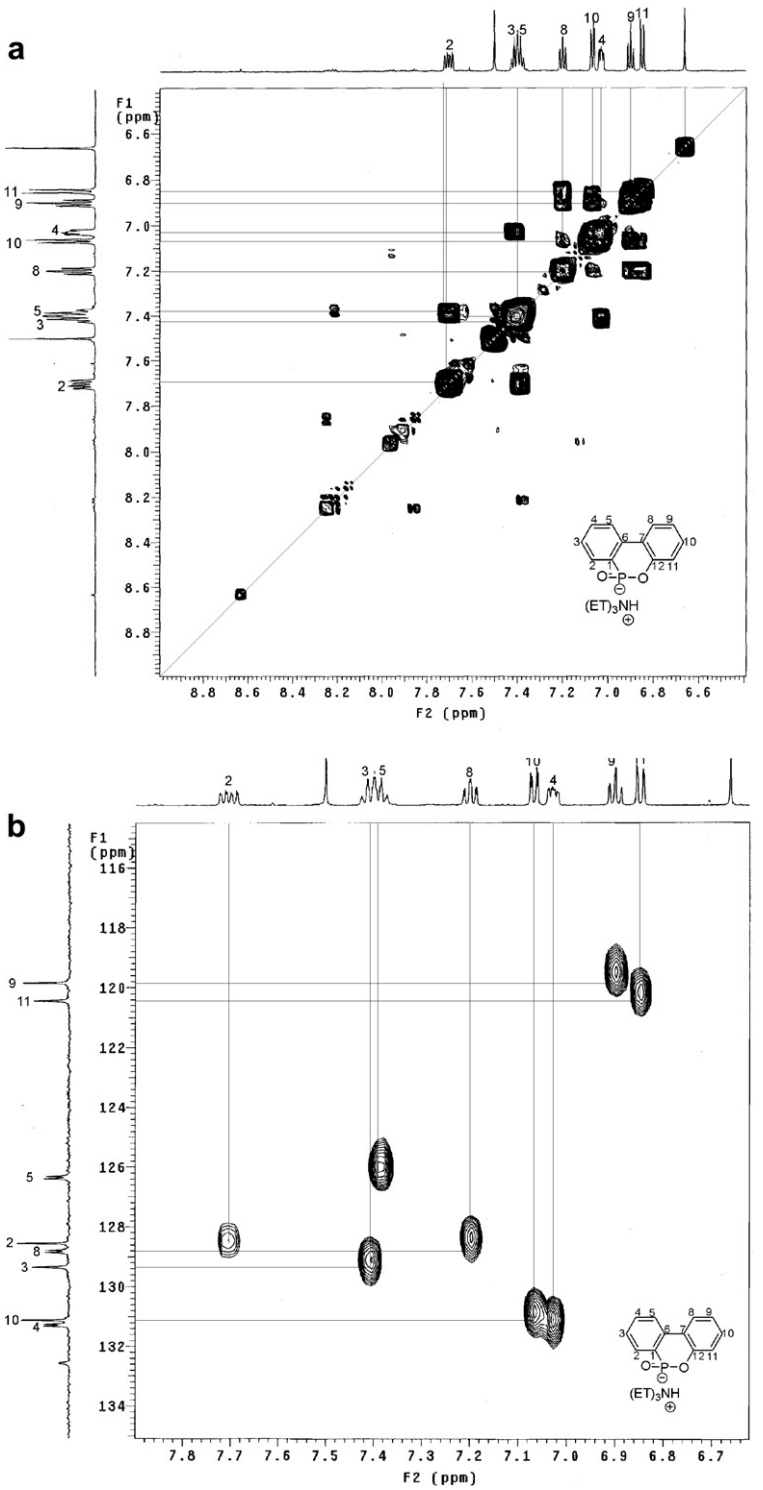

Fig. 2. (a) ^{1}H–^{1}H COSY and (b) ^{1}H–^{13}C HETCOR spectra of the intermediate I.

also reduces the mobility of molecular chains, leading to a higher T_g. According to the literature, when a flame retardant element, such as phosphorus, is introduced into the polymer, T_g of polymer decreases slightly [22] or apparently [23] with the phosphorus content. The T_g-enhanced phenomenon

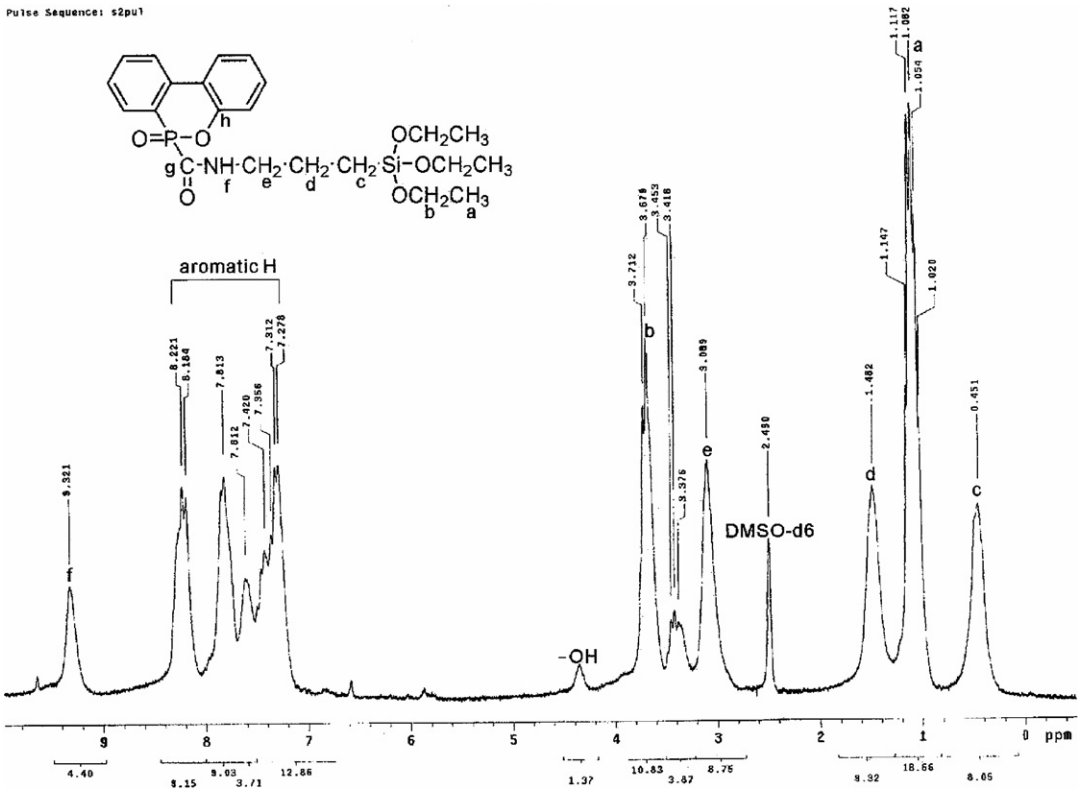

Fig. 3. ^{1}H NMR spectrum of **dopo-icteos**.

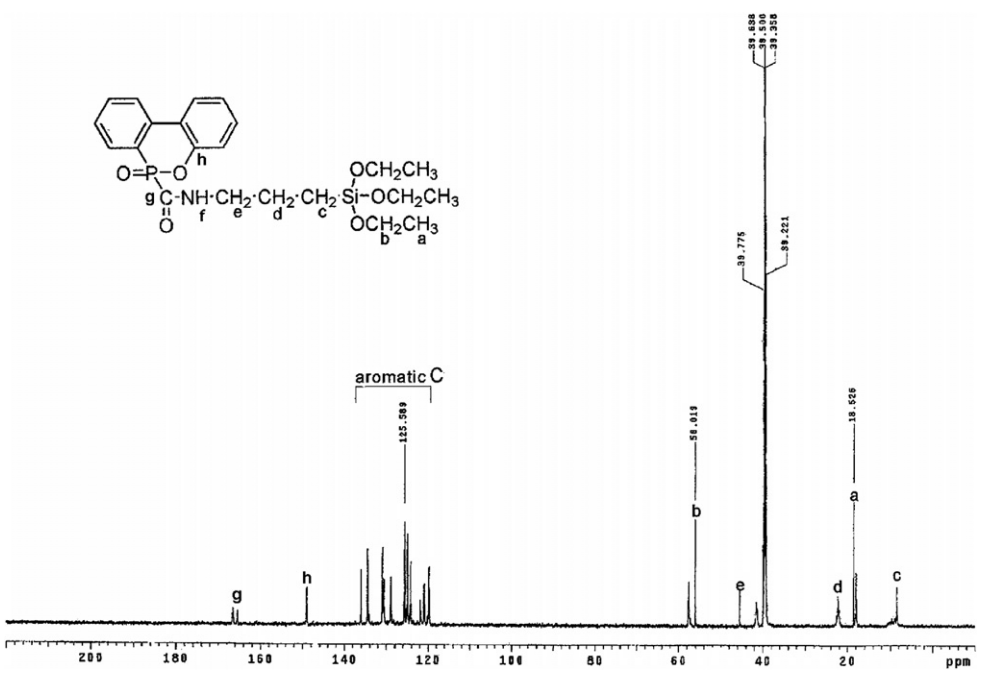

Fig. 4. ^{13}C NMR spectrum of **dopo-icteos**.

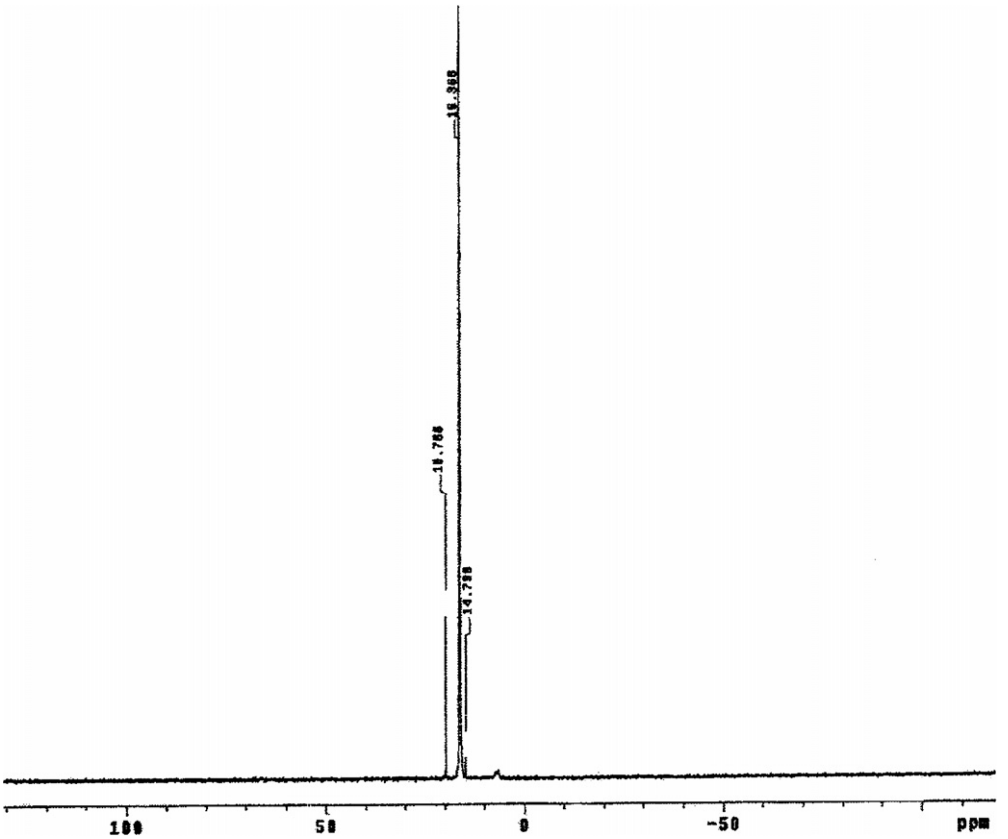

Fig. 5. ^{31}P NMR spectrum of **dopo-icteos**.

is rarely seen in the literature after introducing a phosphorus element into epoxy resin [24]. As to the polyimide/SiO_2 system, no obvious T_g is observed by DSC scans. The rigid structure of the polyimide/SiO_2 hybrids limits the relaxation of polymer chains, resulting in a small and undetectable change and in heat capacity. However, the featureless (no exothermic and endothermic peak) DSC curves for the polyimide/SiO_2 hybrid indicates the gel reaction is almost complete after imidization. Since the T_gs of the polyimide/SiO_2 hybrids are not detectable by DSC scans, DMA was used to measure their T_gs. Fig. 9 shows DMA curve of the polyimide/SiO_2 hybrid, and the results are listed in Table 2. The T_gs of the polyimide/SiO_2 hybrids are in the range of 404–377 °C at a heating rate of 10 °C/min and 384–372 °C at a heating rate of 5 °C/min, decreasing with the content of **dopo-icteos** due to the plasticizing effect of the aliphatic bonds. However, even though the T_g decreases with the content of **dopo-icteos**, the value of 372 °C is high enough for any applications.

3.5. TGA analysis and flame retardancy

TGA traces of polymers provided additional information regarding their thermal stability and thermal degradation behavior. Table 1 lists the thermal stability data of the epoxy/SiO_2 system. The 5% degradation temperatures are in the range of 376–322 °C, decreasing slightly with the amounts of **dopo-icteos**, but higher char yields, increasing from 15% to 26%, were observed. The high flame-retardant phosphorus and silicon elements should be responsible for the increasing char yield. According to the TGA curves, no continuous weight losses below 300 °C corresponding to the release of ethanol and water during heating scans are observed. This indicates the almost completion of the sol–gel reaction. Table 2 lists the thermal stability data of the polyimide/SiO_2 system. The 5% degradation temperatures are in the range of 585–511 °C respectively, also decreasing with the content of **dopo-icteos**. However, the char yield increases from 54% to 63% after incorporating **dopo-icteos**. The lower

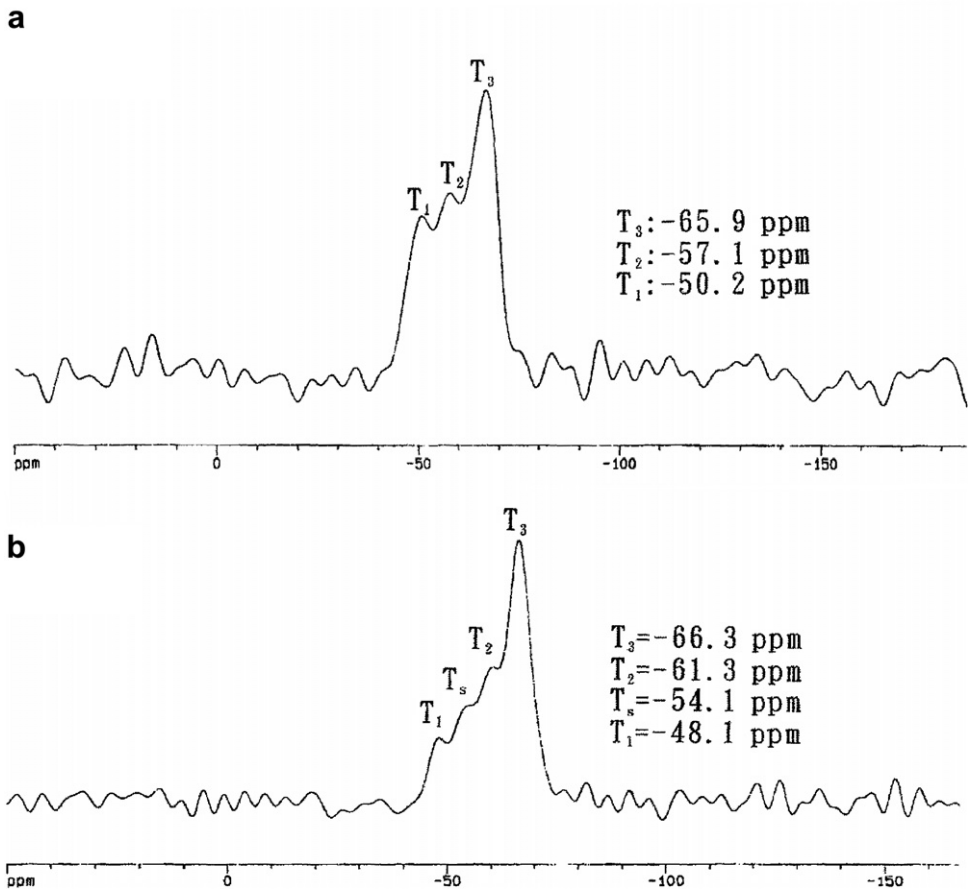

Fig. 6. Solid-state ^{29}Si NMR spectra of (a) epoxy-di10 and (b)epoxy-di20.

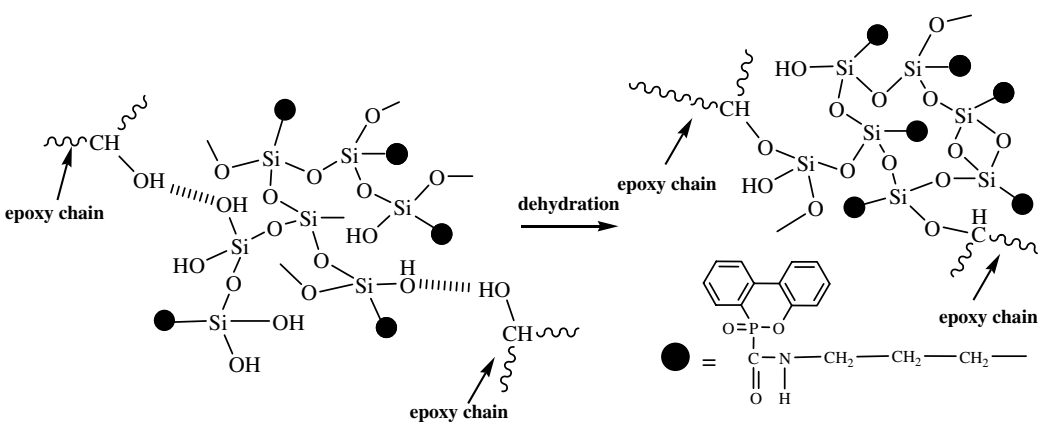

Scheme 5. Dehydration reaction between the hydroxy of epoxy chains and silanol group of silica network.

thermal stability of the aliphatic C–C and P–O bonds in **dopo-icteos** should be responsible for the lower stability of the epoxy/SiO_2 and polyimide/SiO_2 systems. The LOI of the epoxy/SiO_2 hybrids is shown in Table 1. LOI increases from 21 to 28 after incorporating phosphorus and silicon elements, indicating that the flame retardancy is improved. However, the LOI is not very high due to the aliphatic structure in the **dopo-icteos**.

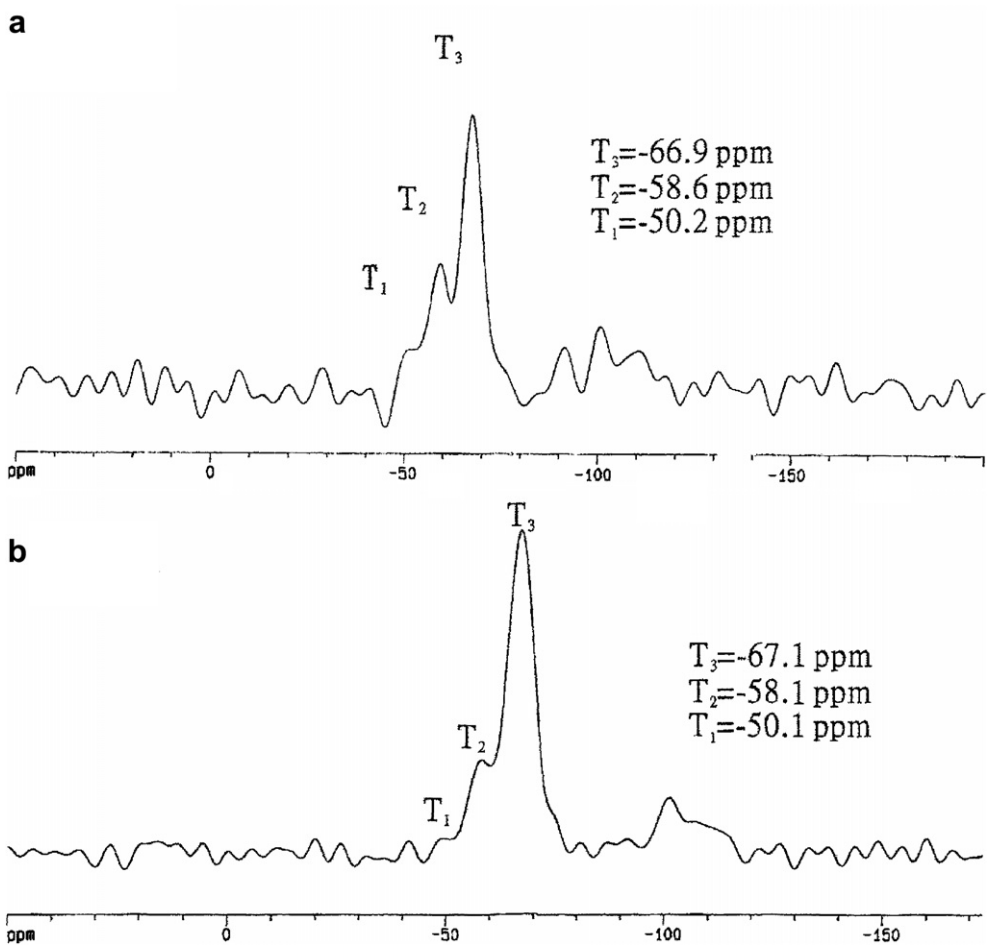

Fig. 7. Solid-state ^{29}Si NMR spectra of (a) pi-di10 and (b) pi-di20.

3.6. Morphology analysis

Since the compatibility between the organic–inorganic hybrids can be judged from the transparency and morphology, the morphologies of the epoxy/SiO_2 and polyimide/SiO_2 hybrids are analyzed by the transparency, SEM and AFM analysis. According to our observation, all the epoxy/SiO_2 hybrids are transparent, even though the oxidation makes the sample a relatively brown color. This indicates good compatibility between silica and epoxy networks; that is, the domain of silica is very small, and no macro phase separation exists. Similar results are observed for the polyimide/SiO_2 system, but the color of the film is darker due to the severe oxidation of polymer chains at higher temperature. Fig. 10 shows the SEM microphotographs of fracture surfaces of the epoxy/SiO_2 hybrids. The domain of silica network is not obvious, showing good compatibility between two phases. The Si and P-mapping of epoxy/SiO_2 with 10% or 20% **dopo-icteos** are shown in Fig. 11. The well dispersed black dots, which stand for the position of the silicon or phosphorus element, further illustrate the homogeneity. Since the compatibility can be increased by the hydrogen bonding between the two phases, the hydrogen bonding between the epoxy network and silica network makes the distribution of silica network more homogeneous, resulting in well-dispersed, small silica domains. Fig. 12 shows the SEM microphotographs of fracture surfaces of the polyimide/SiO_2 system. Unlike the epoxy/SiO_2 system where no obvious silica domain was observed, small well-dispersed silica particles were observed. The number of SiO_2 particles increases with increasing amounts of **dopo-icteos**, but the particle size seems not changed apparently with the content of **dopo-icteos**. The Si-mapping and P-mapping of the polyimide/SiO_2 (not shown here

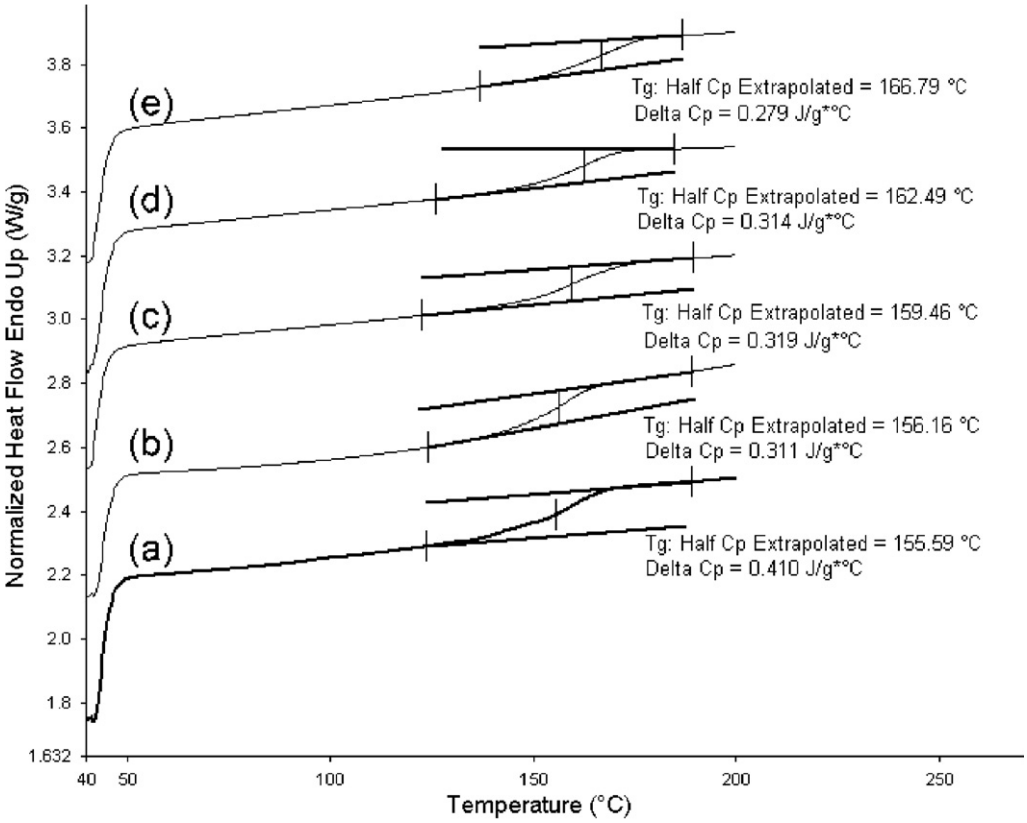

Fig. 8. DSC scans of (a) epoxy-di0, (b) epoxy-di5, (c) epoxy-di10, (d) epoxy-di15 and (e) epoxy-di20.

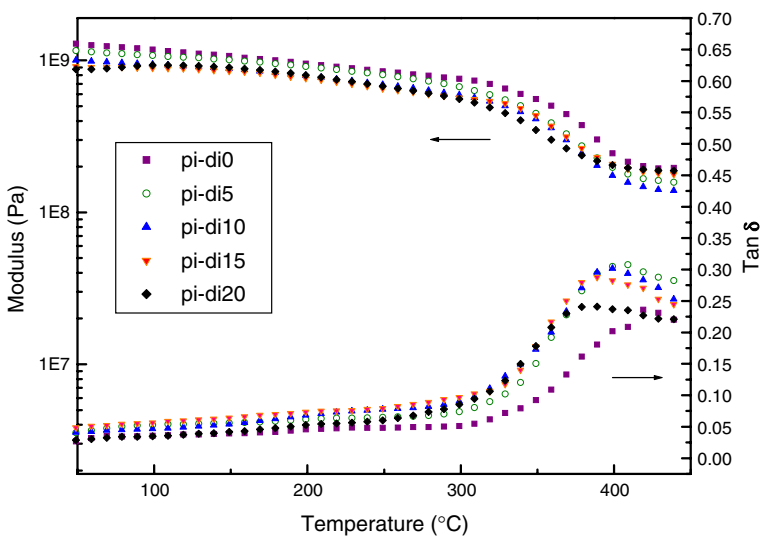

Fig. 9. DMA curves of the polyimide/SiO_2 hybrids at a heating rate of 10 °C/min.

for brief) also show homogeneous dispersion of Si and P elements. The hydrogen boding between the NH and C═O, as shown in Scheme 3, explains the well-dispersion of silica domains. However, unlike the epoxy/SiO_2 system where dehydration between C–OH and Si–OH took place during the curing and

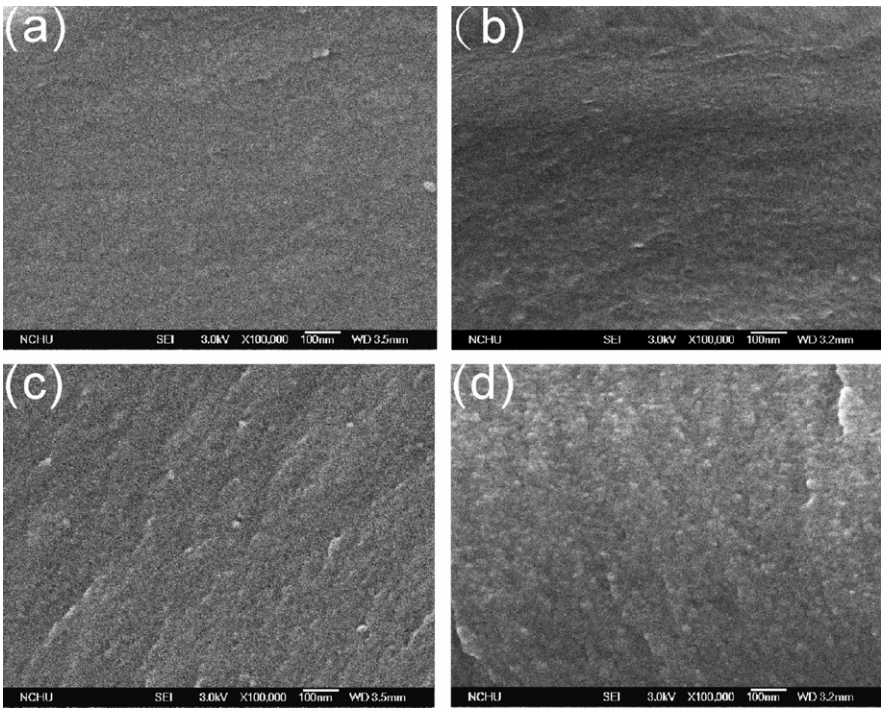

Fig. 10. SEM microphotographs of the fracture surfaces of (a) epoxy-di0, (b) epoxy-di10, (c) epoxy-di15 and (d) epoxy-di20.

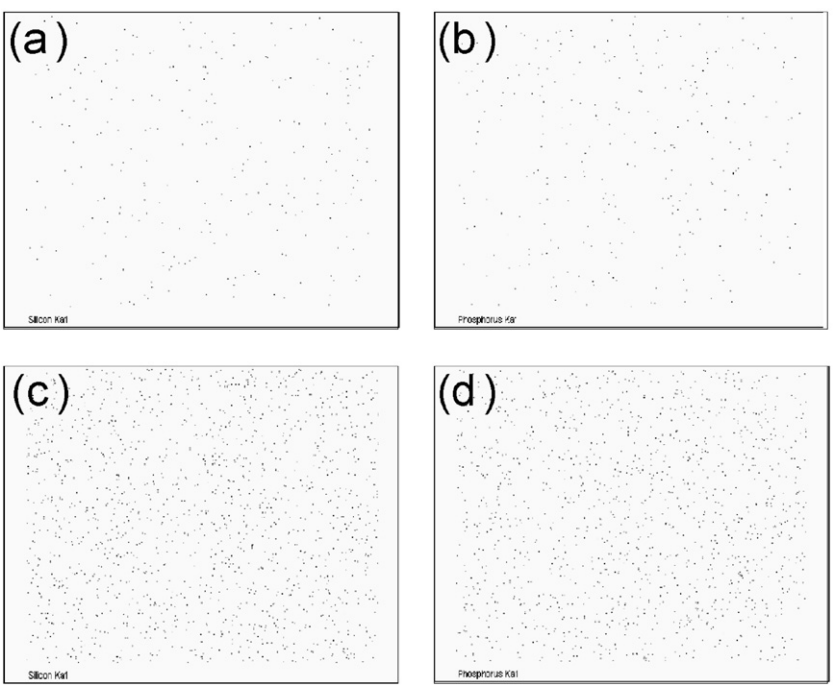

Fig. 11. (a) Si-mapping of epoxy-di10, (b) P-mapping of epoxy-di10, (c) Si-mapping of epoxy-di20 and (d) P-mapping of epoxy-di20.

gel reaction, no chemical bonding exists in the polyimide/SiO_2 system, so the phase difference in the polyimide/SiO_2 system is more obvious than that in the epoxy/SiO_2 system. Fig. 13 shows the AFM

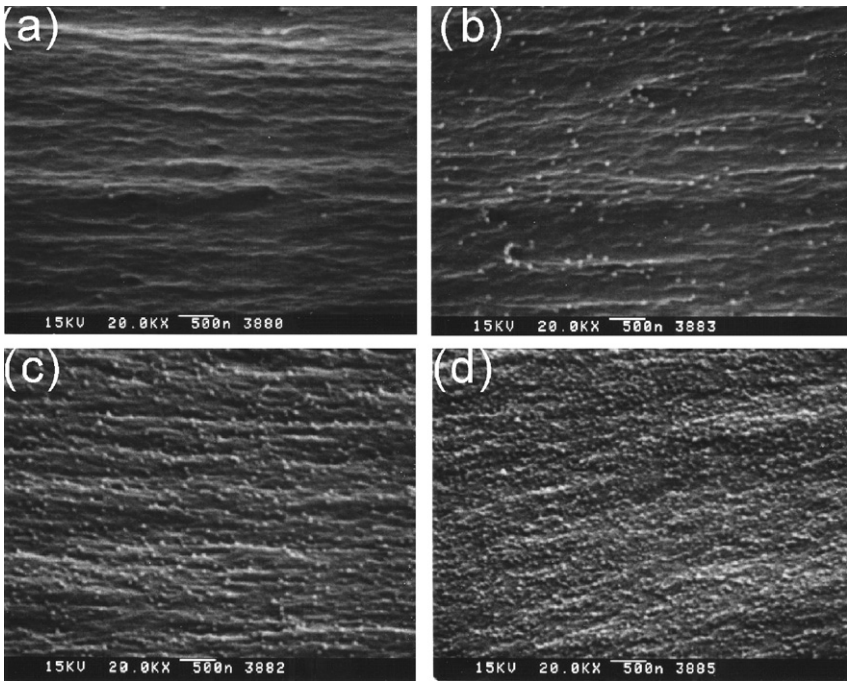

Fig. 12. SEM microphotographs of the fracture surfaces of (a) pi-di0, (b) pi-di5, (c) pi-di10 and (d) pi-di20.

topography, phase image and surface analysis of epoxy-di15. The domain of silica network is also well-dispersed. The dimension of silica network analyzed by AFM surface analysis is around 24 ± 4 nm and 28 ± 5 nm for epoxy-di15 and epoxy-di20 (not shown here), respectively. The AFM topography,

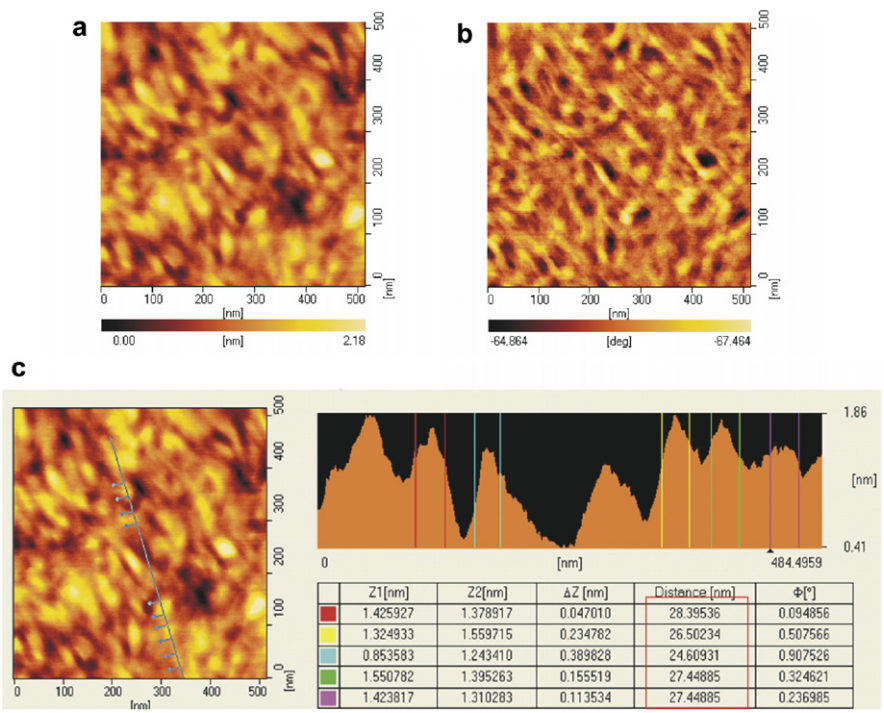

Fig. 13. AFM (a) topography, (b) phase image and (c) surface analysis of epoxy-di15.

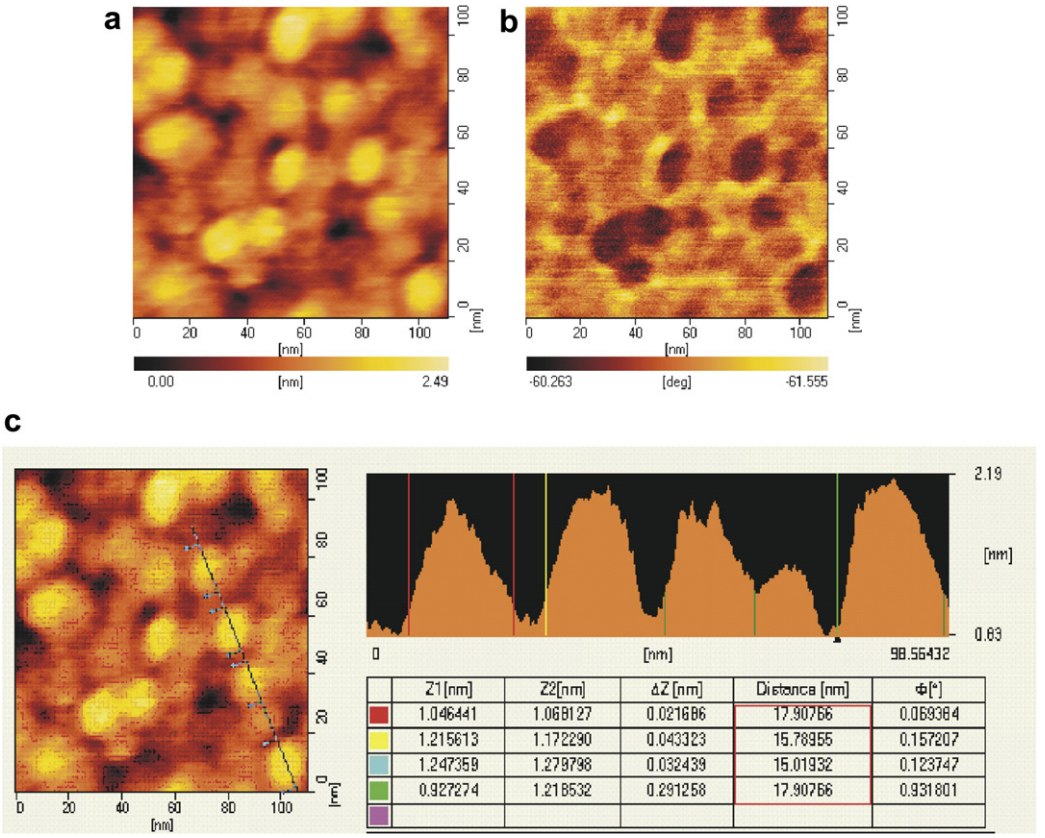

Fig. 14. AFM (a) topography, (b) phase image and (c) surface analysis of pi-di15.

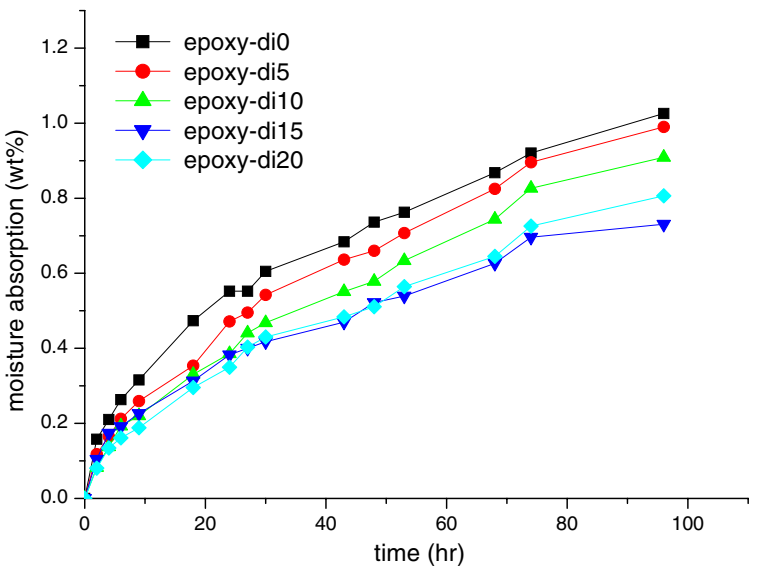

Fig. 15. Moisture absorption curves of the epoxy/SiO_2 hybrids.

phase image and surface analysis of pi-di15 are shown in Fig. 14. The dimension of silica network analyzed by AFM surface analysis is around 15 ± 3 nm for pi-di15 and 17 ± 4 nm for pi-di20

(not shown here). The results of AFM surface analysis indicate the particle size of silica domain in the epoxy/SiO_2 and polyimide/SiO_2 systems is nano scale. There are four carbonyl groups in the repeating unit of polyimide, so the possible hydrogen bonding cite in the polyimide/SiO_2 system is higher than that in the epoxy/SiO_2 system. This makes the distribution of silica network more homogeneous, and thus polyimide/SiO_2 hybrids exhibit smaller silica domain.

3.7. Dielectric and moisture analysis

The signal propagation delay time of integrated circuits is proportional to the square root of dielectric constant of the matrix, and the signal propagation loss is proportional to the square root of dielectric constant and dissipation factor of the matrix. Thus, a material with low dielectric constant and low dissipation factor will reduce the signal propagation delay time and the signal propagation loss. The dielectric constant and dissipation factor of the epoxy/SiO_2 hybrids are shown in Table 1. The dielectric constant is in the range of 3.29–3.16 at 1 GHz, decreasing with the content of **dopo-icteos**. The low moisture absorption characteristic of silica network, complete gel reaction, higher free volume of PSSQ-like silica structure [5] and the bulky biphenylene-phosphinate side group should be responsible for this phenomenon. Fig. 15 shows the moisture absorption curves of the epoxy/SiO_2 hybrids. The moisture absorption decreases with the increasing content of **dopo-icteos**. The low moisture absorption trend is consistent with the characteristic of lower dielectric constant and dissipation factor shown in Table 1.

4. Conclusion

A new phosphorus-containing triethoxysilane, **dopo-icteos**, was successfully synthesized. A triethylamine-catalyzed mechanism was proposed and verified by NMR analyses. Epoxy/SiO_2 polyimide/SiO_2 nanocomposites based on **dopo-icteos** were synthesized successfully. In the epoxy/SiO_2 system, the resulting epoxy/SiO_2 nanocomposites exhibit better char yield, higher glass transition, higher flame retardancy, and lower dielectric constant than those of neat DGEBA/DDM system. ^{29}Si NMR spectra show T^3 (tri-substituted siloxane) was the major microstructure in the network. The SEM images of the fracture surfaces show no obvious phase difference because of the dehydration between hydroxy and silanol groups. AFM surface analysis shows silica domain is smaller than 30 nm. As to the polyimide/SiO_2 system, the Tgs decreases slightly with the content of **dopo-icteos** due to the plasticizing effect of the aliphatic bonds. ^{29}Si NMR spectra show the peak height ratio of T^3/T^2 or T^3/T^1 in the polyimide/SiO_2 is much higher than that in the epoxy/SiO_2 system, indicating that the conversion of gel reaction in the polyimide/SiO_2 system is very high. Unlike the epoxy/SiO_2 system, the polyimide/SiO_2 system shows small well-dispersed silica particles in the SEM images of fracture surfaces. According to the AFM surface analysis, the diameter of silica is around 20 nm, indicating that nanocomposites were achieved.

Acknowledgements

The authors thank the National Science Council of the Republic of China for the financial support. Partial financial support by the Green Chemistry Project (NCHU), as funded by the Ministry of Education, is also gratefully acknowledged.

References

[1] Park J, Jana SC. Polymer 2004;45:7673.
[2] Tyran HL, Leu CM, Wei KH. Chem Mater 2001;13:222.
[3] Tyan HL, Liu YC, Wei KH. Chem Mater 1999;11:1942.
[4] Wahab MA, Kim IL, Ha CS. J Polym Sci Part A: Polym Chem 2004;42:5189.
[5] Tsai MH, Whang WT. Polymer 2001;42:4197.
[6] Shang XY, Zhu ZK, Yin J, Ma XD. Chem Mater 2002;14:71.
[7] Chang CC, Chen WC. Chem Mater 2002;14:4242.
[8] Chen Y, Iroh JO. Chem Mater 1999;11:1218.
[9] Wahab MA, Kim IL, Ha CS. Polymer 2003;44:4705.
[10] Hedrick JL, Cha HJ, Miller RD. Macromolecules 1997;30:8512.
[11] Qiu WL, Luo YJ, Chen FT, Duo YQ, Tan HM. Polymer 2003;44:5821.
[12] Liu YL, Wu CS, Chiu YS, Ho WH. J Polym Sci Part A: Polym Chem 2003;41:2354.
[13] Chiang CL, Wang FY, Ma CCM, Chang HR. Polym Degrad Stab 2002;77:273.
[14] Chiang CL, Ma CCM. Eur Polym J 2002;38:2219.
[15] Yoon CB, Shim HK. Macromol Chem Phys 1998;199:2433.
[16] Lee YJ, Huang JM, Kuo SW, Chen JK, Chang FC. Polymer 2005;46:2320.
[17] Choi J, Yee AF, Laine RM. Macromolecules 2003;36:5666.
[18] Huang J, He C, Liu X, Xu J, Tay CS, Chow SY. Polymer 2005;46:7018.

[19] Hook RJ. J Non-cryst Solids 1996;195:1.
[20] Morikawa A, Iyoku Y, Kakimoto MA, Imai Y. Polym J 1992;24:107.
[21] Liu YL, Wu CS, Hsu KY, Chang TC. J Polym. Sci Part A: Polym Chem 2002;40:2329.
[22] Rwei SP, Liu AY, Liou GS. Polym Eng Sci 2004;44:376.
[23] Lin CH, Cai SX, Lin CH. J Polym Sci Part A: Polym Chem 2005;43:5971.
[24] Cai SX, Lin CH. J Polym Sci Part A: Polym Chem 2005;43: 2862.